atoms

MDPI

Article

A Critical Analysis of Target Ionization and Projectile Electron Loss in Neutral– and Ion–Atom Collisions

Michele A. Quinto [1,*], Nicolás J. Esponda [1], Maria F. Rojas [1], Roberto D. Rivarola [1,2] and Juan M. Monti [1,2]

[1] Instituto de Física Rosario (CONICET-UNR), Bv 27 de Febrero 210 bis, Rosario 2000, Argentina
[2] Laboratorio de Colisiones Atómicas, FCEIA, IFIR, Universidad Nacional de Rosario, Avenida Pellegrini 250, Rosario 2000, Argentina
* Correspondence: quinto@ifir-conicet.gov.ar

Abstract: Electron removal (target ionization and/or projectile electron loss) in neutral–atom collisions is theoretically studied for the impact of H^0, He^0 and He^+ beams on noble gases (He, Ne and Ar). These reactions are investigated theoretically within the Continuum Distorted Wave-Eikonal Initial State model. New features have been included in the theoretical model: (i) a scaled projectile charge depending on its velocity and charge, (ii) a dynamic projectile-effective-charge depending on the momentum transfer, and (iii) a dynamic target-effective-charge depending on the kinematics of the emitted electron. The energy and angular spectra of emitted electrons from the target and from the projectile are calculated and compared with the available experimental data. Also, the influence of each one of the corrections on the resulting spectra will be studied.

Keywords: CDW-EIS; neutral–atom; electron removal

Citation: Quinto, M.A.; Esponda, N.J.; Rojas, M.F.; Rivarola, R.D.; Monti, J.M. A Critical Analysis of Target Ionization and Projectile Electron Loss in Neutral– and Ion–Atom Collisions. *Atoms* **2023**, *11*, 149. https://doi.org/10.3390/atoms11120149

Academic Editor: Sabyasachi Kar

Received: 25 September 2023
Revised: 15 November 2023
Accepted: 16 November 2023
Published: 21 November 2023

1. Introduction

In atomic collisions, electron removal processes are of fundamental interest considering that they involve the ionization of the aggregates. These reactions are fundamental for understanding the physics and nature of matter. In different branches of Science such as thermonuclear fusion, auroras, stopping power, and radiobiology, among others, the knowledge of such mechanisms is relevant to describe several physical phenomena. When a bare projectile (a nuclear charge) impacts an atomic or molecular target, the electron production comes only from the target. However, in successive collisions, a bare projectile can capture electrons from the targets and also lose them in subsequent interactions. These collisional systems are more complex to investigate. On one hand, as the projectile is no longer a single charged particle, its potential is not a pure-Coulomb one. On the other hand, the multiple processes can involve both target and projectile electrons, e.g., simultaneous ionization of the target and the projectile or the ionization of one of the aggregates together by the simultaneous excitation of the other one.

Bates and Griffing did pioneer work investigating collisions involving dressed projectiles [1], using the first-order Born approximation in order to describe the simple collision system of neutral hydrogen impacting on a hydrogen atom. One of the most interesting results obtained was that in addition to single inelastic (SI) processes, double inelastic (DI) reactions were also available. The SI process considers that the projectile or the target remains frozen while the other aggregate is ionized. The DI event takes into account the projectile or target excitation with the ionization of the other centre and also the simultaneous ionization of both aggregates. Over the years different investigations dealt with these types of collisions, both theoretically and experimentally. Jakubassa et al. [2] have computed Double Differential Cross-Sections (DDCSs) of electron loss in asymmetrical collisions like Ne and Ar targets interacting with neutral hydrogen. The theoretical cross-sections were calculated within the Electron Impact Approximation (EIA) since the electron was considered as a quasi-free particle in the target potential. Later on, Hartley et al. [3]

employed the Impulse Approximation (IA) and the first-order Born approximation (FBA) for describing SI and DI events, respectively. They computed DDCSs for neutral hydrogen and partially charged projectiles (He^+ and O^{4+}) colliding with Ar targets, showing some discrepancies with the experiments mainly due to the limitation of the FBA to describe the reactions. Dubois et al. [4] have calculated DDCSs within the Plane Wave Born approximation (PWBA) to represent measurements of He^+ impact on atoms and molecules (He, Ar and H_2O). In that work, four different channels were analyzed: single target ionization, target ionization with simultaneous projectile excitation, single projectile ionization, and projectile ionization with simultaneous target excitation. The dressed projectile charge was considered as a dynamic one depending on the momentum transfer in order to take into account the screening produced by the projectile electrons. Heil and coworkers [5] reported several measurements and theoretical results of DDCSs related to electron emission in dressed-atom collisions. The measurements were performed in coincidence with the projectile charge allowing them to distinguish the contribution of the projectile electrons from those of the target. The PWBA model was used to compute the DDCSs describing adequately the SI events, whereas it was shown that a higher-order Born approximation was necessary to represent the DI processes. In the same context, Kuzel et al. [6] have performed measurements for asymmetrical systems such as neutral hydrogen and helium beams impacting on Ar atoms. The electron spectra were measured in coincidence with the projectile charge to discern from which aggregate the electrons were ejected. A second-order Born approximation was employed to describe the DI events, namely when both the target and projectile were ionized or excited in one collision step. Following the work Jakubassa et al. [2], Jalowy et al. [7] have investigated both theoretically, within the EIA approximation, and experimentally the electron loss by light projectiles with Ne. The authors have pointed out the importance of DI reactions in the collisional systems investigated. The inclusion of these contributions improves significantly the agreement between theory and experiments for all the energies and angles.

The present work aims to describe the SI events in asymmetrical collisions: neutral hydrogen and neutral and singly charged helium impact on noble gases: He, Ne and Ar. It should be mentioned that the CDW-EIS model has been largely employed to describe the single ionization process in the ion–atom collisions, where numerous works have shown its effectiveness [8–10]. We will present an extension of the quantum mechanical Continuum Distorted Wave-Eikonal Initial State (CDW-EIS) approximation to the case of the dressed and partially dressed projectiles. In order to extend the CDW-EIS model to the present study, three corrections are considered: (i) a scaled projectile charge depending on its velocity and charge, (ii) a dynamic projectile-effective-charge depending on the momentum transfer, and (iii) a dynamic target-effective charge depending on the kinematics of the emitted electron. For these collision systems, at the first stage, we focus our interest only on the SI processes: target ionization and projectile electron loss. The theoretical calculations in terms of TCSs, SDCSs and DDCSs are compared with other theoretical models and the available experimental data.

Atomic units (a.u.) are used throughout unless indicated otherwise.

2. Theory

2.1. Single Target Ionization by Dressed Projectiles

The Continuum Distorted Wave-Eikonal Initial State approximation is employed to describe the electron removal from the target and projectile. In the multi-electronic target case, the CDW-EIS model considers an effective target with a single active electron assuming that the other target electrons (the passive ones) remain frozen in their initial orbitals during all the collision. Therefore, within the independent electron model and following the procedure given in [8,10,11], the multi-electronic Hamiltonian can be reduced to a single-active-electron one given by

$$H_e = -\frac{1}{2}\nabla^2 + V_T(\boldsymbol{x}) + V_P(\boldsymbol{s}) + V_S(\boldsymbol{R}) \quad (1)$$

where $\boldsymbol{x}$ and $\boldsymbol{s}$ represent the active electron position in the reference frame fixed to the target and the projectile, respectively. While the potential $V_T(\boldsymbol{x})$ includes the interaction of the active electron with the rest of the target, the term $V_P(\boldsymbol{s})$ describes the interaction between the target active electron and the projectile, and $V_S(\boldsymbol{R})$ accounts for the interaction between the projectile with the target nucleus and its passive electrons.

Within the straight-line version of the impact parameter approximation, the $V_S(\boldsymbol{R})$ potential gives rise to a phase factor that will affect the multiple differential cross-sections depending on the projectile scattering angle. As the Double Differential Cross-Sections (DDCSs) do not depend on the projectile scattering angle, that term will be neglected in the following analysis [11–13].

The first-order of the *prior* version of ionization transition amplitude within the CDW-EIS approximation can be written as

$$\mathcal{A}_{if}^{-}(\boldsymbol{\rho}) = -\mathrm{i}\int_{-\infty}^{\infty} dt \left\langle \chi_f^{-} \middle| \left(H_e - \mathrm{i}\frac{\partial}{\partial t} \right) \middle| \chi_i^{+} \right\rangle \tag{2}$$

where the initial and final distorted wave functions (χ_i^{+}, and χ_f^{-}, respectively) are proposed as

$$\chi_i^{+}(\boldsymbol{x}, \boldsymbol{s}, t) = \Phi_i(\boldsymbol{x}, t)\mathcal{L}_i^{+}(\boldsymbol{s}) \tag{3}$$
$$\chi_f^{-}(\boldsymbol{x}, \boldsymbol{s}, t) = \Phi_f(\boldsymbol{x}, t)\mathcal{L}_f^{-}(\boldsymbol{s}) \tag{4}$$

with $\Phi_i(\boldsymbol{x}, t) = \phi_i(\boldsymbol{x})\exp(i\epsilon_i t)$ and $\Phi_f(\boldsymbol{x}, t) = \phi_f(\boldsymbol{x})\exp\left(i\epsilon_f t\right)$ the initial-bound and final-continuum wave function solutions of the time-dependent Schrödinger equation, and ϵ_i and ϵ_f the corresponding electron energies, respectively.

The target final-continuum state $\phi_f(\boldsymbol{x})$ is chosen as a hydrogenic continuum function defined as

$$\phi_f(\boldsymbol{x}) = \frac{1}{(2\pi)^{3/2}}\exp(i\,\boldsymbol{k}\cdot\boldsymbol{x})\,N^*(\lambda)\,{}_1F_1[-i\,\lambda, 1, -i\,(kx + \boldsymbol{k}\cdot\boldsymbol{x})] \tag{5}$$

with $\epsilon_f = k^2/2$ the final electron energy, being $\boldsymbol{k}$ the ejected electron momentum in the target reference frame. The term $N(a) = \exp(\pi a/2)\Gamma(1 - ia)$ (with Γ being the Euler's Gamma function) is the normalization factor of the ${}_1F_1$ hypergeometric function, and $\lambda = \tilde{Z}_T/k$ with $\tilde{Z}_T$ being an effective charge. In general, this charge is chosen according to Belkić's criteria, $\tilde{Z}_T = \sqrt{-2n^2\epsilon_i}$, with ϵ_i the orbital energy and n the principal quantum number of the atomic orbital [12]. The continuum function given by (5) corresponds to approximating the potential $V_T(\boldsymbol{x})$ by an effective Coulomb potential $\left(-\tilde{Z}_T/x\right)$ in the exit channel. In this work, we will adopt the recent development introduced in the CDW-EIS model by Rojas et al. [14], where the $\tilde{Z}_T$ is described by a dynamic charge depending on the energy and angle of the emitted electron. This charge is defined as

$$\tilde{Z}_T(\theta_e, E_e) = \mathbf{B}(t) \tag{6}$$

where $\mathbf{B}(t)$ is a Bézier function (see Equation (15) of Ref. [14]). For small angles, $\tilde{Z}_T$ tends to the Belkić's charge, whereas for backscattering angles $\tilde{Z}_T$ goes to the target nuclear charge (for more details see [14]). This correction improves the CDW-EIS double differential cross-sections for backward emission angles.

For dressed projectiles, $V_P(s)$ is a non-Coulomb potential that is approximated in the work of Monti et al. [10] by a two-parameter analytic independent-particle Green–Sellin–Zachor (GSZ) model potential [15]. This potential can be written as a Coulomb long-range term plus a short-range one, given by:

$$V_P(s) = -\frac{q}{s} - \frac{1}{s}(Z_P - q)\Omega(s) \tag{7}$$

with $\Omega(s) = [H(\exp(s/d) - 1) + 1]^{-1}$. The H and d parameters depend on the projectile nuclear charge Z_P and its degree of ionization q. These values of H and d are tabulated in [15].

The initial and final channel distortions are chosen as

$$\mathcal{L}_i^+(\boldsymbol{s}) = \exp[-\mathrm{i}\nu \ln(vs + \boldsymbol{v}.\boldsymbol{s})] \tag{8}$$

$$\mathcal{L}_f^-(\boldsymbol{s}) = N^*(\zeta)\,{}_1F_1[-\mathrm{i}\zeta; 1; -\mathrm{i}(ps + \boldsymbol{p}.\boldsymbol{s})] \tag{9}$$

where $\boldsymbol{v}$ is the projectile velocity, $\nu = q/v$, $\boldsymbol{p} = \boldsymbol{k} - \boldsymbol{v}$ is the electron momentum in the projectile reference frame. In the final channel distortion, Equation (9), the parameter $\zeta = \tilde{q}(\mathbf{K})/p$ is chosen following the recent work by Esponda et al. [16], where $\tilde{q}(\mathbf{K})$ is a dynamic projectile charge depending on the momentum transfer $\mathbf{K}$. Such charge is written as

$$\tilde{q}(\mathbf{K}) = Z_P - F(\mathbf{K}) \tag{10}$$

with $F(\mathbf{K})$ being the projectile form factor [17]. For small momentum transfer $\tilde{q}(\mathbf{K})$, tends to $Z_P - N$, whereas for large momentum transfer $\tilde{q}(\mathbf{K})$, goes to Z_P, therefore even for neutral projectiles (with $q = 0$) the final channel distortion never vanishes [16].

The scattering amplitude is then expressed as the sum of two terms: the first one corresponding to the long-range Coulomb term and the second one corresponding to the contribution of the short-range part of the potential [10]

$$\mathcal{A}_{if}^-(\boldsymbol{\rho}) = \mathcal{A}_{if}^{-(a)}(\boldsymbol{\rho}) + \mathcal{A}_{if}^{-(s)}(\boldsymbol{\rho}). \tag{11}$$

By employing the Fourier transform, the $\mathcal{A}_{if}^-(\boldsymbol{\rho})$ can be expressed as a function of the transverse momentum transfer $\boldsymbol{\eta}$

$$\mathcal{R}_{if}^-(\boldsymbol{\eta}) = \int d\boldsymbol{\rho} \exp(i\boldsymbol{\rho}.\boldsymbol{\eta}) \mathcal{A}_{if}^-(\boldsymbol{\rho}). \tag{12}$$

This allows calculating the cross-sections using the $\mathcal{R}_{if}^-(\boldsymbol{\eta})$ for which analytical expression can be obtained [18]. For ionization by bare projectiles, $\mathcal{A}_{if}^{-(s)}(\boldsymbol{\rho}) = 0$, since only the Coulomb contribution affects the transition amplitude. In the case of dressed projectiles, both terms must be considered.

The doubly differential cross-sections are given by

$$\frac{d^2\sigma_{if}}{dE_e d\Omega_e} = k \int d\boldsymbol{\eta} |\mathcal{R}_{if}^-(\boldsymbol{\eta})|^2, \tag{13}$$

where E_e is the emission energy, and Ω_e the solid angle subtended by the emission angle θ_e. Then, by numerical integration of the DDCS (13) over the emission energy, we access the SDCS as a function of the emission angle. Finally, the TCS is computed by further integrating the SDCS over the emission angle.

2.2. Projectile Electron Loss

The electron loss process can be addressed by reversing the role of the collision aggregates and using Lorentz transformations of target and projectile reference frames [19]. We noticed that the $\tilde{q}(\mathbf{K})$ introduced by Esponda et al. in [16] may lead to enlarge the influence of the projectile on the ionized electron. More precisely, the ELC peak in the backward direction in the laboratory frame could be underestimated (see Figure 1c).

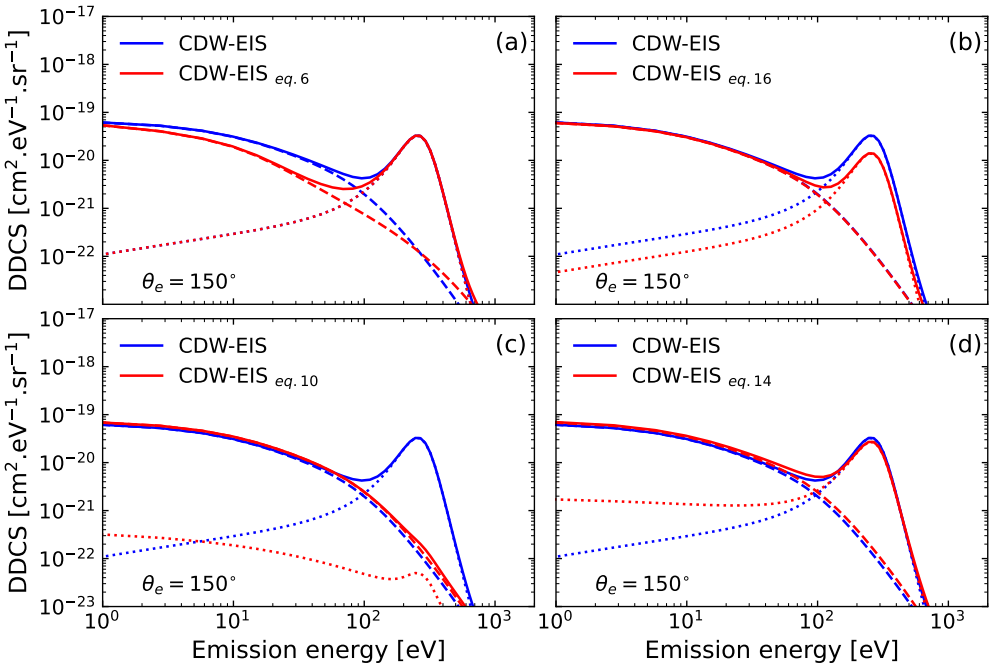

Figure 1. DDCS for electron emission in H^0–Ar at 500 keV/u as a function of electron emitted energy for a fixed θ_e = 150° emission angle. In each sub-figure, the effect of each correction is shown in contrast with the usual CDW-EIS *prior* from [10]. Dashed line: target ionization; dotted line: projectile electron loss; full line: total electron emission. CDW-EIS with correction by Equation (6) (**a**); CDW-EIS with correction by Equation (16) (**b**); CDW-EIS with correction by Equation (10) (**c**) and CDW-EIS with correction by Equation (14) (**d**).

This behaviour is more noticeable in asymmetrical systems, for large emission angles in the laboratory frame. This leads us to suppose that the perturbation introduced into the final channel strongly influences the dynamic of the collision. Therefore, in order to investigate the mentioned dependence with the emitted electron angle, we propose to include in the projectile dynamic charge a simple factor $f(\theta_e)$ depending on the emission angle in the laboratory frame θ_e:

$$\tilde{q}(\mathbf{K}, \theta_e) = f(\theta_e)(Z_P - F(\mathbf{K})) \tag{14}$$

with $f(\theta_e)$ a linear function:

$$f(\theta_e) = 1 - \theta_e/180, \tag{15}$$

where θ_e is given in degrees.

Considering Equation (15) into (14) diminishes the projectile perturbation into the final channel as the emission angle, θ_e, increases. We do that using a simple approach with the help of a linear function. The aim of this correction is to recover at least the results obtained with the First Born approximation (see Figure 1d). We remember that in a neutral–atom collision, the CDW-EIS approximation reduces to First Born approximation [16].

Now, we also introduce a correction due to the relationship between the projectile charge and its velocity. For a bare projectile, the validity of the perturbative theory could be estimated by Sommerfeld's factor, Z_P/v. When the projectile charge increases the validity of these models moves towards the high-collision-energy region. Then, in order to extend the validity of the theory towards the low-energy region, hence keeping a reasonable

accuracy for mid- and low-collision energies, we introduced a re-scaling of the projectile potential. We propose a simple formula inspired by the Bezt's model [20]:

$$\bar{V}_P(s) = \alpha(v, Z_P) V_P(s) \quad (16)$$

$$\alpha(v, Z_P) = 1 - \exp\left(-v/\sqrt{Z_P}\right) \quad (17)$$

In Figure 2 it can be seen that the correction introduced by Equations (16) and (17) will affect cross-sections for collision energies lower than 1 MeV/u.

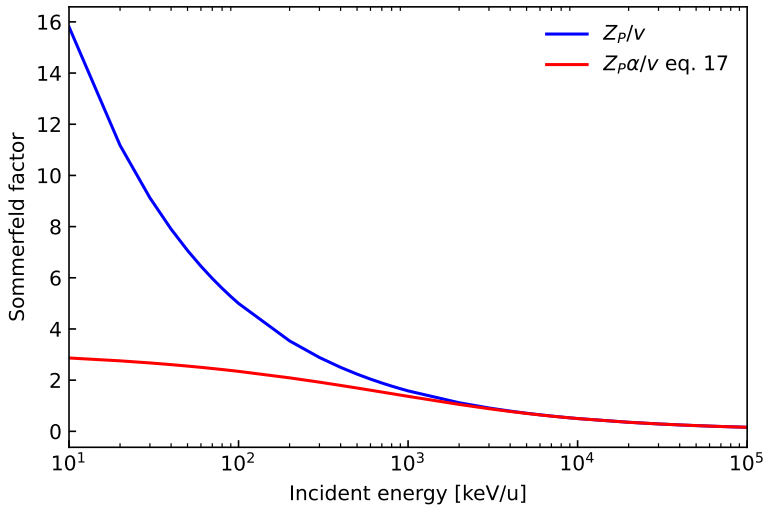

Figure 2. Sommeferld factor Z_P/v (blue line) and $Z_P\alpha/v$ (red line) (with α given by Equation (17)) as a function of the projectile incident energy for $Z_P = 10$.

2.3. Influence of Present Corrections

We analyze the individual influence of each of the three corrections implemented in the CDW-EIS approximation. The three corrections introduced are the dynamic target-effective-charge Equation (6), the scaled projectile potential Equation (16) and the dynamic projectile-effective-charge Equation (14).

In Figures 1 and 3 the contributions of each correction with respect to the CDW-EIS version from [10] are presented for two emission angles $\theta_e = 150^\circ$ and $\theta_e = 30^\circ$. The dynamic target-effective-charge from Equation (6) depends on the electron emission energy and angle. This correction affects only the target ionization DDCS for the backscattering region (see Figures 1a and 3a). The scaled projectile potential correction depends on the charge and velocity of the projectile; the resulting DDCSs are affected by a factor equal to $\alpha^2(v, Z_P)$ (see Figures 1b and 3b). The last correction is the dynamic projectile-effective-charge. This correction is defined by Equation (10) and was initially introduced in [16]. For forward emission (see Figures 3c), we observe that this correction slightly increases the target ionization cross-section, since the two center effects of the collision are recovered (see [16]). When this correction is employed for the projectile electron loss we observe a reduction of the ELC peak at forward emission and a more significant reduction for backward emission (see Figure 1c). In the latter case, the ELC peak is underestimated. This could be due to an overestimation of the projectile form factor which leads to a larger projectile screening the more noticeable for a projectile with low q and high number of electrons. To deal with this problem, we have proposed a modification of the Equation (10) in order to reduce the effect of the projectile distortion in the final channel in the backscattering region. Thus, the dynamic projectile-effective-charge correction is now defined by Equation (14), which allows us to recover qualitatively the ELC peak for backward emission (see Figure 1d).

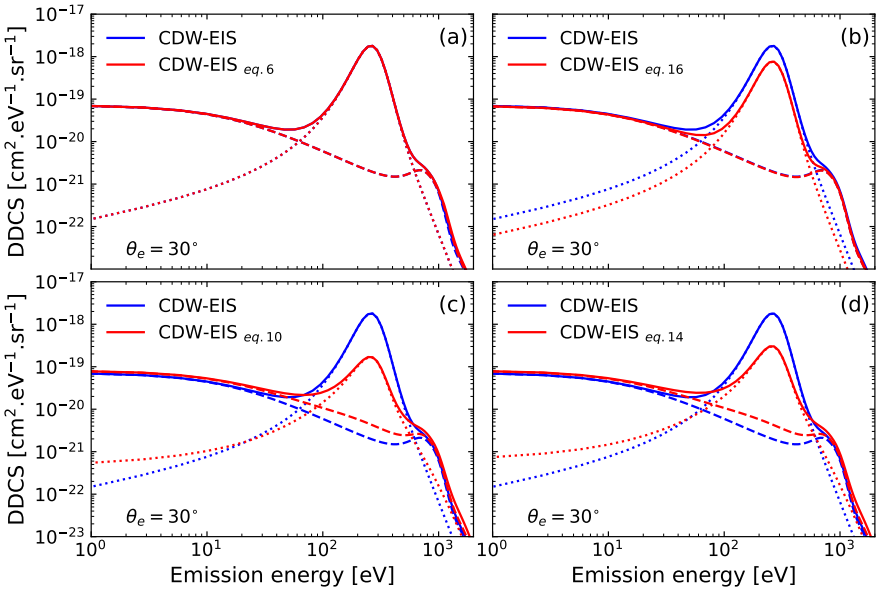

Figure 3. Same as Figure 1 but for $\theta_e = 30^\circ$ emission angle. CDW-EIS with correction by Equation (6) (**a**); CDW-EIS with correction by Equation (16) (**b**); CDW-EIS with correction by Equation (10) (**c**) and CDW-EIS with correction by Equation (14) (**d**).

3. Results

We report the theoretical cross-sections and compare them with existing experimental data. The theoretical calculations were computed within the CDW-EIS approximation from [10] and the present CDW-EIS-v2. They include only the SI events, namely, target ionization and projectile electron loss. The present results (CDW-EIS-v2) are obtained by considering the three corrections stated above: the dynamic target-effective-charge, Equation (6), the scaled projectile-potential, Equation (16) and dynamic projectile-effective-charge, Equation (14). The following collision systems are investigated: H^0–, He^+– and He^0– impact on Neon and Argon noble gases. Also, for the sake of completeness, we show in Appendix A the DDCSs of Ne target impacted by H^0–, He^+– and He^0 at 500 keV/u.

3.1. DDCS

In Figure 4 we show the DDCSs for electron emission in 500 keV/u H^0–Ar collision as a function of emitted electron energy for a given fixed emission angle in the laboratory reference frame. Four fixed emission angles have been investigated, $\theta_e = 30^\circ$, 90°, 150° and 180°. It can be observed that target ionization clearly dominates over the projectile electron loss in the low-energy part of the spectra for all emission angles, whereas the intermediate emission energy region (electron momentum close to the projectile velocity) is dominated by the ELC-peak electrons. Also, at $\theta_e = 30^\circ$, the binary peak structure is observed, and then it vanishes for larger emission angles. It is evident that the ionization of the target is only slightly affected by the corrections given that, in this case, the projectile is H^0. The largest modification is observed in the electron loss case in which the H^0 atom is ionized by the Ar one. It is also noticeable that CDW-EIS-v2 results (also CDW-EIS for large emission angles) tend to underestimate the experimental ELC peak of a factor equal to 10 at $\theta_e = 180^\circ$. For comparison, the results of DDCSs computed within the IA theory by Wang et al. [21] and the EIA theory by Kuzel et al. [6] for SI are reported. Also, the DDCSs as the sum of SI + DI given by the theory of Kuzel et al. [6] are depicted. As mentioned by the authors, the theories IA and EIA were developed specifically to describe the electron emission in ELC peak region [6,21].

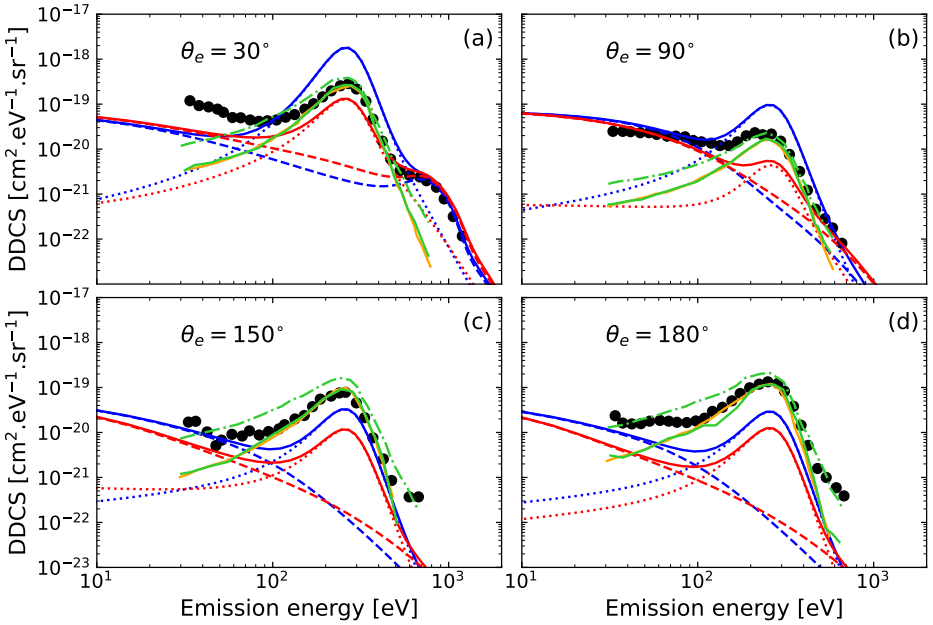

Figure 4. DDCS for electron emission in H^0–Ar collision at 500 keV/u as a function of electron energy. Theories: SI (orange line) theory of [21]; SI (green line) and SI + DI (dashed-dot green line) theory of [6]; CDW-EIS (blue lines) and CDW-EIS-v2 (red lines). Target ionization (dashed lines), projectile electron loss (dotted lines), and the sum of both (solid lines). Experimental data given by [6]. Observed emission angles $\theta_e = 30^\circ$ (**a**); $\theta_e = 90^\circ$ (**b**); $\theta_e = 150^\circ$ (**c**) and $\theta_e = 180^\circ$ (**d**).

In Figure 5, we show DDCSs for the electron emission in 100 keV/u He^0–Ne collision as a function of emitted electron energy. Four emission angles have been investigated, θ_e = 40°, 90°, 120° and 160°. As the collision energy is low, this case presents a less pronounced ELC-peak structure than the one observed in the 500 keV/u H^0–Ar, even though the angles are not exactly the same. This is observed in both experimental data and theoretical results. At this impact energy, 100 keV/u, when considering the electron loss process, the CDW-EIS approximation starts to be less accurate as it moves away from the limit of the perturbative regime. For comparison, the results of DDCSs computed within the EIA by Jalowy et al. [7] for SI and the sum of SI + DI are depicted. We observe that for emission angle, $\theta_e = 90^\circ$, the CDW-EIS-v2 results are in accord with those of the EIA theory. For forward emission, the SI results given by EIA theory are in accord with the experiment. For backward emission, the SI DDCSs give a reasonable agreement with the experiment for an emission energy greater than 100 eV. However, when the DI processes are included, we observe an overestimation of the EIA results with respect to the measurements.

In Figure 6, the theoretical DDCSs are depicted for He^0– and He^+–Ar collisions, left and right panels, respectively. In general, we observe a qualitative good agreement between the theory and experiments, as was shown in the case of H^0–Ar collision. Although, for backward emission, in the He^0 case, an underestimation is found in the ELC peak. The SI results given by the EIA theory given by Kuzel et al. [6] show good agreement with the measurements. We observe that when DI is summed up to SI, the EIA results largely overestimate the experiments. The CDW-EIS-v2 model improves mainly the electron loss process in the ELC region for forward angle emission. For He^+–Ar collisions at $\theta_e = 150^\circ$, the dynamic $\tilde{Z}_T$ (Equation (6)) slightly enhances the target ionization. Also, the present calculations are in agreement with PWBA results (SI + DI) given by DuBois et al. [4]. For $\theta_e = 30^\circ$, the PWBA results slightly overestimate the experimental in ELC peak. Whereas, for $\theta_e = 130^\circ$, the PWBA results differ from the measurements for emission energy less than 30 eV.

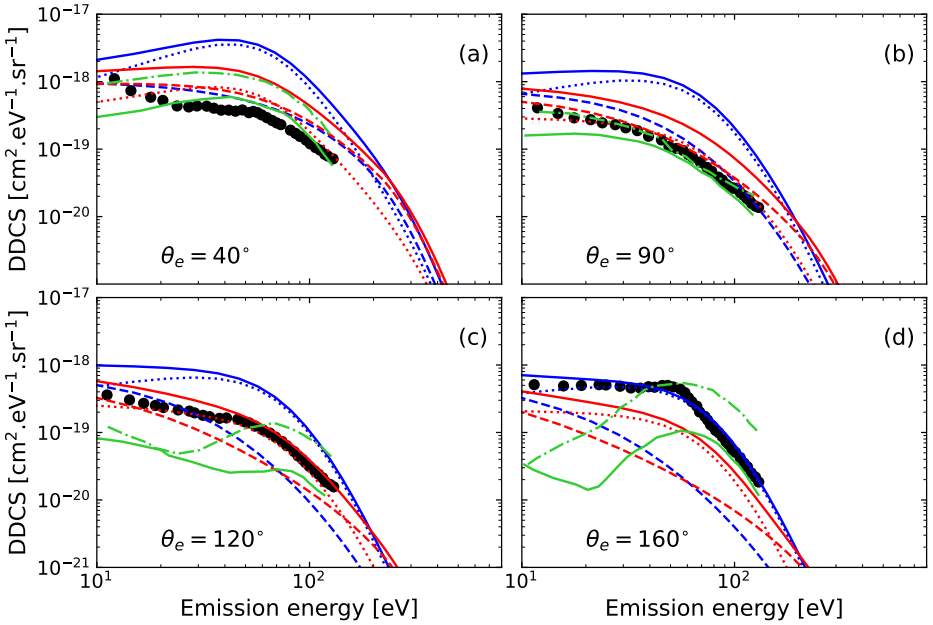

Figure 5. DDCSs for electron emission in He^0–Ne collision at 100 keV/u as a function of electron energy. Theories: SI (green line) and SI + DI (dashed-dot green line) theory of [7]; CDW-EIS (blue lines) and CDW-EIS-v2 (red lines). Target ionization (dashed lines), projectile electron loss (dotted lines) and the sum of both (solid lines). Experimental data given by [7]. Observed emission angles $\theta_e = 40°$ (**a**); $\theta_e = 90°$ (**b**); $\theta_e = 120°$ (**c**) and $\theta_e = 160°$ (**d**).

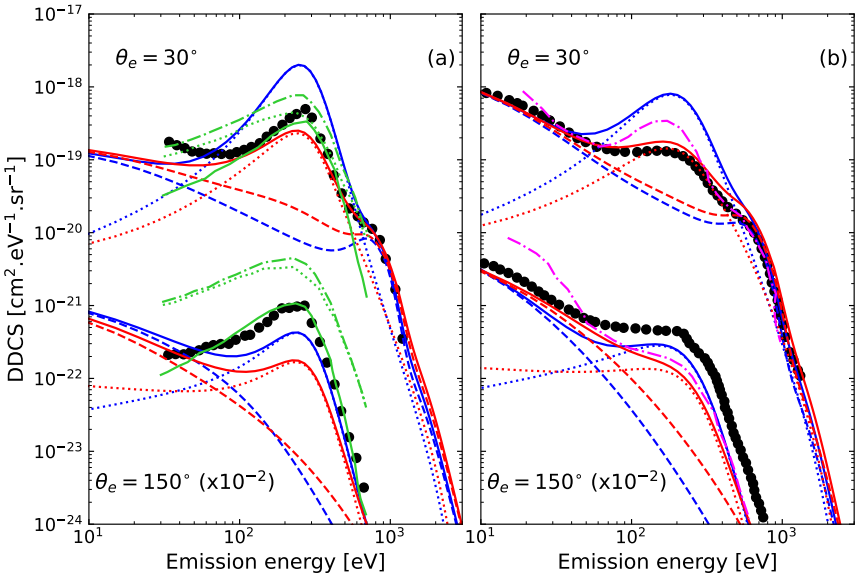

Figure 6. DDCS for electron emission in He^0–Ar collision at 500 keV/u (**a**) and in He^+–Ar collision at 400 keV/u (**b**) as a function of emission energy. Theories: SI (green line), DI (dotted green line) and SI + DI (dashed-dot green line) theory of [6]; SI + DI (dashed-dot magenta line) theory of [4]; CDW-EIS (blue lines) and CDW-EIS-v2 (red lines). Target ionization (dashed lines), projectile electron loss (dotted lines) and the sum of both (solid lines). Experimental data given by [6] (**a**) and [4] (**b**).

In Figure 7, we present the DDCSs for electron emission as a function of emission angle for Argon impacted by He^{2+}, He^+ and He^0 projectiles at 300 keV/u and 500 keV/u collision energies. The theoretical results for 250 eV electron emission energy are compared with the experimental data (only for the case of He^{2+} and He^+ impact) of Toburen et al. [22]. The CDW-EIS-v2 cross-sections show a qualitatively good agreement with respect to the

measurement for most of the angular spectra. We observe that the magnitude of DDCSs, for the three projectiles, converge in the binary peak angle. Also, for the 500 keV/u collision energies, the DDCSs increase in magnitude as the emission angle goes toward 0° reaching their maximum. This is due to the fact that the DDCSs are computed for an electron emission energy equal to 250 eV, which gives an electron momentum close to projectile velocity. Therefore, as the emission angle goes to zero, the increase of the DDCS for He^{2+} projectiles is due to the ECC peak, whereas for He^{+} and He^{0} it corresponds to the sum of both the ECC peak and ELC one [16].

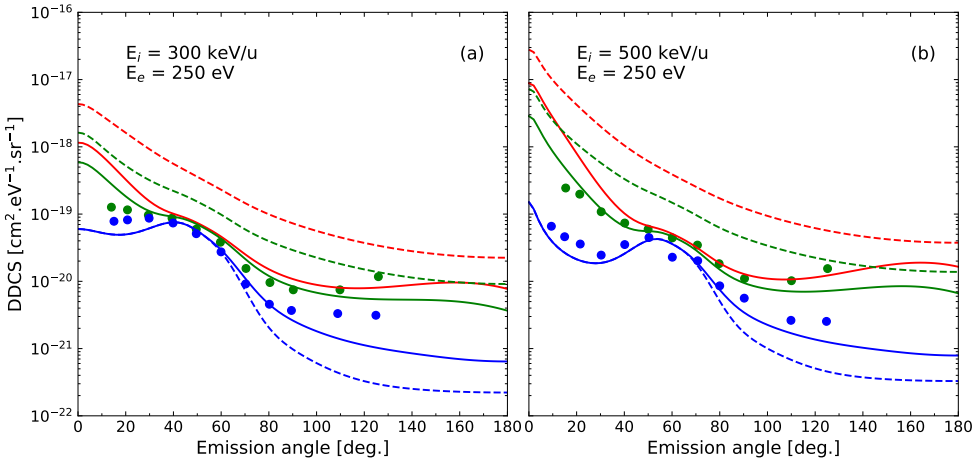

Figure 7. DDCS for electron emission in He^{0} (red lines), He^{+} (green lines), and He^{2+} (blue lines) impinging on Ar at 300 keV/u (**a**) and 500 keV/u (**b**) as a function of emission angle. Theoretical DDCSs: CDW-EIS (dashed lines) and CDW-EIS-v2 (solid lines). Experimental data given by [22]: He^{+} (green circles) and He^{2+} (blue circles).

3.2. SDCS

From the experimental DDCSs (see Figures 4 and 5), we remark that initially the ELC peak decreases in magnitude with increasing the emission angle, its shape becomes more rounded, and it then reaches a minimum around 90°. After that, the ELC peak starts increasing its magnitude reaching a maximum at 180°. This feature produces the Ramsauer–Townsend effect [7,23]. This effect was investigated by Jalowy et al. [7] for the 0.1 MeV/amu He^{0}–Ne collisions. Due to the DI processes, they found that the measured SDCSs showed a large enhancement of the electrons released for angles above 100°.

For the case of weakly bounded electrons, the projectile electron loss process could be studied within the scattering theories of a free electron interacting with a spherical target-potential [6,23]. Therefore, for comparison, we have included in Figure 8, where theoretical calculations and measurements in terms of SDCSs as a function of emission angle are reported, the elastic scattering cross-section for e^{-}–He, Ne and Ar collision system computed at the same projectile velocities. The electron SDCSs were calculated with the PW theory by ELSEPA code [24], and these cross-sections show the Ramsauer-Townsend structure. The latter is more evident in the e^{-}–Ne and Ar collisions (Figure 8b,c). The theoretical SDCSs were obtained by integrating the DDCSs in the energy range corresponding to the ELC peak. The Ramsauer–Townsend effect is less notable in the CDW-EIS results. In the case of H^{0} projectiles (Figure 8a,b), the CDW-EIS-v2 calculations show a remarkable agreement with the experiment in the angular range between 0° and 90°. Then, in the backscattering region, the theoretical results SDCSs underestimate the experimental data, although showing a qualitative trend according to the measurements. This underestimation comes from the discrepancy observed in the DDCSs for large scattering angles, namely, at 150° and 180° (see Figure 4), in the energy spectrum of the electron loss process. In Figure 8c, the He^{0}–Ne collisional system is presented. The CDW-EIS-v2 calculations show a qualitative accord with the experiments. However, an overestimation of a factor 2 is

observed in forward emission. For backward emission, we find the same behavior as in the other cases. For comparison, the results from other theories have also been included.

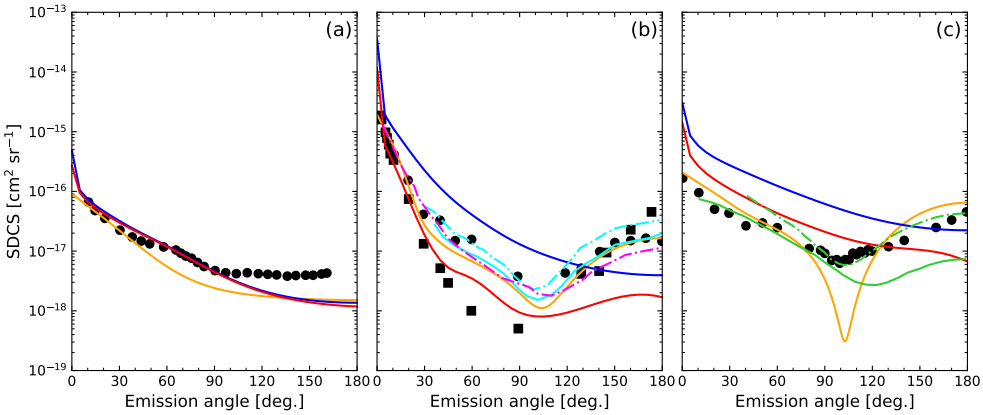

Figure 8. SDCSs for electron emission in 150 keV/u H^0–He (**a**), 500 keV/u H^0–Ar (**b**), and 100 keV/u He^0–Ne (**c**) as a function of electron emitted angle. Theories: SI (green line) and SI + DI (dashed-dot green line) theory of [7]; SI (magenta line) theory of [21]; SI (cyan line) and SI + DI (dashed-dot cyan line) theory of [6]; CDW-EIS (blue lines); CDW-EIS-v2 (red lines) and PW elastic electron scattering at equally projectiles velocity computed with ELSEPA [24] (orange lines). Experimental data given by [25] (**a**), [6] (**b**) and [7] (**c**).

3.3. TCS

The experimental cross-sections, reported for the presented collisional systems, are deduced from the measurements of σ_+ and σ_-, representing the total production of positive ions and electrons, respectively [26–35]. Also, we compare with the measurements of Santos et al. for He^+ [36] and Sarkadi et al. for H^0 [37], who have performed the measurements by coincident technique.

3.3.1. Target Ionization

In Figures 9 and 10 we show the TCSs of Ne and Ar ionization, respectively, impacted by H^0, He^0 and He^+. In Figure 9a, in case of H^0–Ne collision, the computed TCSs underestimate by a factor of about 2 the measurements reported by Green and McNeal [28]. Also, it can be observed that the theoretical results are in good agreement with the measurements of Sarkadi et al. [37]. Whereas, for the Ar target, (see Figure 10a) a large discrepancy is shown between the theory and the experimental results of Green and McNeal [28] and Sarkadi et al. [37]. Furthermore, the two sets of measurements, reported for H^0–Ne and –Ar collisions, are inconsistent between them. For He^+ impact on Ne and Ar atoms, we observe that the theoretical TCSs give a qualitative accordance with the experimental data (see Figures 9c and 10c). For comparison, we report the Born and SLPA theoretical TCSs given by Miraglia et al. [9]. In the case of He^+–Ne, we observe that the Born results are in accord with the CDW-EIS ones in the pertubative regime. Also, the SLPA and CDW-EIS-v2 results are in concordance between them for an impact energy greater than 200 keV (see Figure 9c). Whereas, in this case of He^+–Ar, we note that the Born and SLPA calculations are qualitatively in agreement with the CDW-EIS and CDW-EIS-v2 ones, respectively, in the perturbative regime (see Figure 10c). It should further be noted that no experimental data was found for target ionization by He^0 impact, hence only comparisons between theoretical results are shown in Figures 9b and 10b.

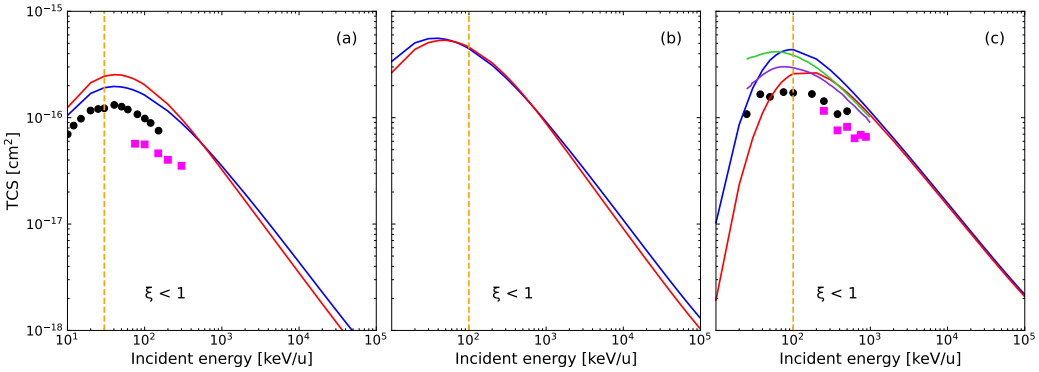

Figure 9. TCSs for target ionization cross-section of Ne impacted by H^0 (**a**), He^0 (**b**) and He^+ (**c**). Theories: Born (green line) and SLPA (violet line) [9]; CDW-EIS (blue lines) and CDW-EIS-v2 (red lines). Experimental data are given by circles [28], squares [37] (**a**); and circles [34], squares [36] (**c**). The vertical dashed line indicates the beginning of the perturbative region, where $\xi = \frac{Z_P}{v} < 1$.

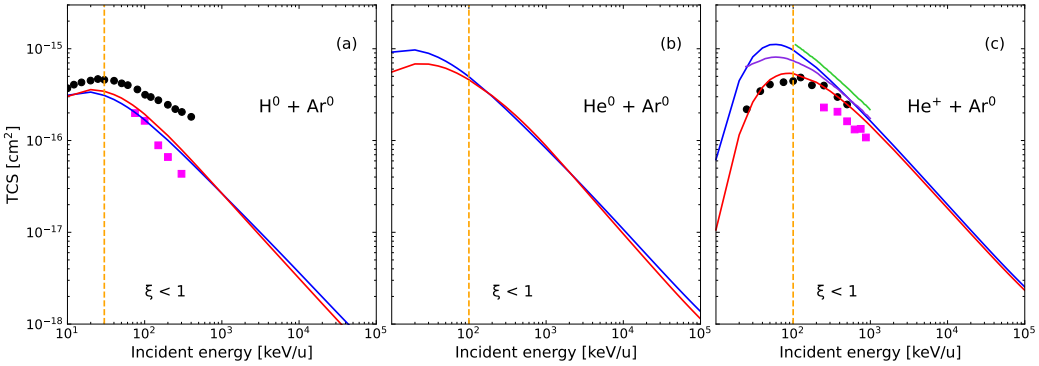

Figure 10. TCSs for target ionization cross-section of Ar impacted by H^0 (**a**), He^0 (**b**) and He^+ (**c**). Theories: Born (green line) and SLPA (violet line) [9]; CDW-EIS (blue lines) and CDW-EIS-v2 (red lines). Experimental data are given by circles [28], squares [37] (**a**); and circles [34], squares [36] (**c**). The vertical dashed line indicates the beginning of the perturbative region, where $\xi = \frac{Z_P}{v} < 1$.

3.3.2. Projectile Electron Loss

In general, the present theoretical calculations, considering the corrections (CDW-EIS-v2), describe well the SI events in the energy impact range presented. Besides, due to the large asymmetry in the collision systems, the corrections have a significant influence over the electron loss process (see Figures 11 and 12). In all presented cases, we observe a remarkable accordance between theories and experiments for impact energy greater than 500 keV. For comparison, the theoretical calculations done with the FCM theory are depicted in all the presented systems [38]. The FCM cross-sections show a good accordance with the various experimental data sets. For the case of H^0 and $He^{0,+}$ interacting with Ne atoms (see Figure 11), the CDW-EIS-v2 theory shows much better agreement with experiments than CDW-EIS. In the case of H^0 and He^0, the improvement is about a factor 10 for low collision energies, whereas for the He^+ one, the improvement is about a factor 3 for low collision energies.

In Figure 12, the total cross-sections for the electron loss process are shown for H^0 and $He^{0,+}$ projectiles impinging on Ar atoms. We observe that the CDW-EIS-v2 largely improves the agreement with experiments when compared to those obtained with CDW-EIS. For the H^0 case, see Figure 12a, the CDW-EIS-v2 results slightly underestimate the measurements in the energy range between 10–300 keV/u. Whereas for the He^0 case, see Figure 12b, the CDW-EIS-v2 results are in quite good agreement with experiments over all the collision energy range. Finally, Figure 12c shows electron loss from He^+ projectiles interacting with Ar targets. In this case, both theories are in agreement with

experiments for collision energies larger than 10^4 keV/u. Nonetheless, for lower collision energies the results obtained with CDW-EIS-v2 are in much better agreement than the ones corresponding to CDW-EIS.

In all the cases presented, even when the agreement between the CDW-EIS-v2 theory with experiments is not excellent, it is clear that there is a major improvement with respect to CDW-EIS that allows us to extend the applicability of the theory to the low-collision-energies domain.

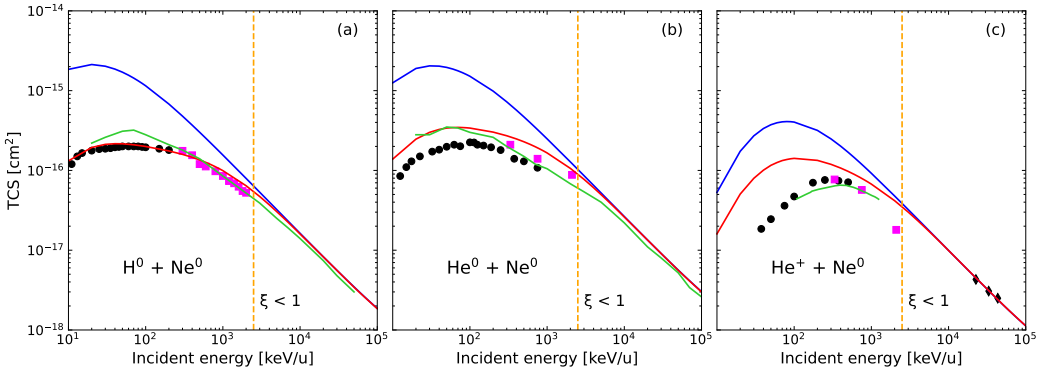

Figure 11. TCSs for projectile electron loss cross-section in Ne impacted by H^0 (**a**), He^0 (**b**) and He^+ (**c**). Theories: FCM (green line) [38]; CDW-EIS (blue lines) and CDW-EIS-v2 (red lines). Experimental data are given by circle [26], squares [33] (**a**); circles [32], squares [30] (**b**); and circles [34], squares [32] diamond [39] (**c**). The vertical dashed line indicates the beginning of the perturbative region, where $\xi = \frac{Z_P}{v} < 1$.

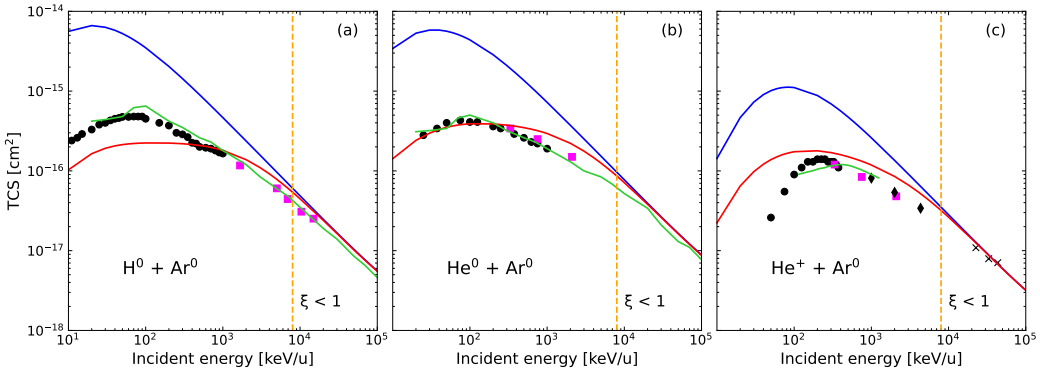

Figure 12. TCSs for projectile electron losscross-sectionn in Ar impacted by H^0 (**a**), He^0 (**b**) and He^+ (**c**). Theories: FCM (green line) [38]; CDW-EIS (blue lines) and CDW-EIS-v2 (red lines). Experimental data are given by circles [26] square [35] (**a**); circles [29], squares [32] (**b**); and circles [27], squares [31], diamonds [32], crosses [39] (**c**). The vertical dashed line indicates the beginning of the perturbative region, where $\xi = \frac{Z_P}{v} < 1$.

4. Discussion

Throughout this work, we have considered asymmetrical collision systems where the target is much larger than the projectile. For these types of systems target ionization evidences small corrections, whereas the projectile electron loss shows major improvement, mainly in the forward direction, when the corrections are included. However, for the case of H^0–Ar collision, we have observed important discrepancies in the DDCSs in the ELC peak for large emission angles as the theoretical DDCSs largely underestimate the measurements. Whereas, for forward emission, the deviation between CDW-EIS-v2 results and the experiment is most likely due to not considering the DI events, for example, the projectile electron loss with target excitation [6]. The DI processes are out of the scope of the present work. The aim is to study these processes in mid-term terms.

The improvements shown in the DDCSs are also evidenced in the SDCS. We have found that for the collision systems investigated a large improvement is observed with respect to previous CDW-EIS calculations. Nonetheless, there are still discrepancies with experimental results, mostly for large laboratory frame emission angles, where an underestimation is found in all presented cases.

In the case of TCSs, there is a major amelioration in the agreement with experimental data in the low-collision-energy range, for both target ionization and projectile electron loss. As stated above, as the collision systems are asymmetrical, improvements are the largest in the case of projectile electron loss. This improvement is largely due to the consideration of the scaled projectile potential factor given in Equation (16). This correction allows us to reduce the lower-collision-energy limit and it permits the calculation of TCS on the region where the Sommerfeld's factor is greater than 1.

5. Conclusions

Electron emission from the target or projectile in neutral– and ion–atom collisions was investigated within the CDW-EIS approximation. Three corrections have been included in the theoretical calculations, namely: (i) the scaled projectile potential, (ii) the dynamic projectile-effective-charge and (iii) the dynamic target-effective-charge. The influence of these corrections has been studied in the presented DDCSs, SDCSs, and TCSs. In general, we found that the corrections improve the agreement with existing experimental data, observing a qualitative amelioration in the differential cross-sections and a better accordance in the total cross-sections for the investigated systems. In the future, DI processes will be the object of our investigations. Also, a more complex dependence of the projectile form factor with the emitted electron dynamic, e.g., by also taking into account the emitted electron energy, could lead to a better description of the dressed-projectile–target-electron interaction.

Author Contributions: Conceptualization, M.A.Q. and J.M.M.; methodology, M.A.Q. and J.M.M.; software, M.A.Q., J.M.M., N.J.E. and M.F.R.; validation, M.A.Q., J.M.M., N.J.E. and M.F.R.; formal analysis, M.A.Q. and J.M.M.; investigation, M.A.Q., J.M.M., N.J.E. and M.F.R.; resources, R.D.R.; data curation, M.A.Q., J.M.M. and R.D.R.; writing—original draft preparation, M.A.Q. and J.M.M.; writing—review and editing, M.A.Q., J.M.M., R.D.R., N.J.E. and M.F.R.; visualization, M.A.Q. and J.M.M.; supervision, R.D.R.; project administration, R.D.R.; funding acquisition, R.D.R. All authors have read and agreed to the published version of the manuscript.

Funding: This research was funded by Consejo Nacional de Investigaciones Científicas y Técnicas de la República Argentina grant number PIP 2021-3245.

Data Availability Statement: Data is contained within this article.

Acknowledgments: The results presented in this work have been obtained using the facilities of the CCT–Rosario Computational Center, a member of the High–Performance Computing National System (SNCAD, MincyT–Argentina) http://cluster.rosario-conicet.gov.ar (accessed on 20 November 2023).

Conflicts of Interest: The authors declare no conflict of interest.

Abbreviations

The following abbreviations are used in this manuscript:

CDW-EIS	Continuum Distorted Wave-Eikonal Initial State
FBA	First Born Approximation
PWBA	Plane Wave Born Approximation
EIA	Electron Impact Approximation
IA	Impulse Approximation
PW	Plane Wave
SLPA	Shell-wise Local Plasma Approximation
FCM	Free Collision Model
DDCS	Double Differential Cross-Section

SDCS	Single Differential Cross-Section
TCS	Total Cross-Section
ECC	Electron Capture to Continuum
ELC	Electron Loss to Continuum
SI	Single Inelastic
DI	Double Inelastic

Appendix A. Analysis for Different Projectiles Impact

In Figure A1, we present the total electron emission, which is the sum of both target ionization and projectile electron loss, for H^0–, He^0–, and He^+–Ne at 500 keV/nucleon impact energy. The DDCSs computed with the CDW-EIS-v2 model describe qualitatively well the experimental data. Even if, for He^0 case, discrepancies are observed between theory and measurements. The ELC peak position is respected in all presented collision systems.For comparison, the DDCS for SI and the sum of SI+DI, computed with IA theory by Jalowy et al. [7], have been depicted for the collisional system He^+–Ne.

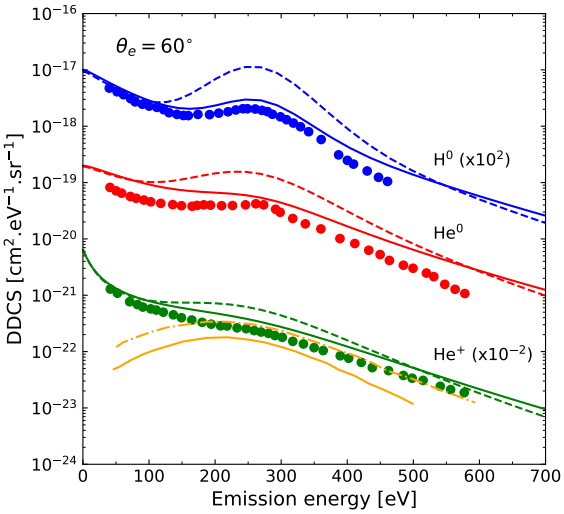

Figure A1. DDCS for electron emission in H^0–(blue), He^0–(red), and He^+–(green) Ne at 500 keV/nucleon as a function of emission energy. Theories: SI (orange line) and SI + DI (dashed-dot orange line) theory of [7]; CDW-EIS (dashed lines), CDW-EIS-v2 (solid lines). Experimental data given by [7].

References

1. Bates, D.R.; Griffing, G.W. Inelastic Collisions between Heavy Particles II: Contributions of Double-Transitions to the Cross Sections associated with the Excitation of Hydrogen Atoms in Fast Encounters with other Hydrogen Atoms. *Proc. Phys. Soc. Sec. A* **1954**, *67*, 663. [CrossRef]
2. Jakubassa, D.H. Electron loss from medium-energy projectiles in collisions with heavy target atoms. *J. Phys. B At. Mol. Opt. Phys.* **1980**, *13*, 2099. [CrossRef]
3. Hartley, H.M.; Walters, H.R.J. Doubly differential cross sections for electron loss. *J. Phys. B At. Mol. Opt. Phys.* **1987**, *20*, 3811. [CrossRef]
4. Dubois, R.D.; Manson, S.T. Electron emission in He^+-atom and He^+-molecule collisions: A combined experimental and theoretical study. *Phys. Rev. A* **1990**, *42*, 1222–1230. [CrossRef]
5. Heil, O.; Dubois, R.D.; Maier, R.; Kuzel, M.; Groeneveld, K.O. Ionization in fast-neutral-particle-atom collisions: H and He atoms impacting on He. *Phys. Rev. A* **1992**, *45*, 2850–2858. [CrossRef]
6. Kuzel, M.; Heil, O.; Maier, R.; Lucas, M.W.; Jakubassa-Amundsen, D.H.; Farmery, B.W.; Groeneveld, K.O. The doubly inelastic contribution to electron loss: H^0 and He^0 (0.5 MeV u^{-1}) in collision with Ar. *J. Phys. B At. Mol. Opt. Phys.* **1992**, *25*, 1839–1851. [CrossRef]
7. Jalowy, T.; Jakubaßa-Amundsen, D.H.; Lucas, M.W.; Groeneveld, K.O. Momentum spectroscopy of electrons lost by light projectiles in collisions with neon targets. *Phys. Rev. A* **2000**, *61*, 022714. [CrossRef]
8. Fainstein, P.D.; Ponce, V.H.; Rivarola, R.D. Two-centre effects in ionization by ion impact. *J. Phys. B At. Mol. Opt. Phys.* **1991**, *24*, 3091–3119. [CrossRef]
9. Miraglia, J.E.; Gravielle, M.S. Ionization of He, Ne, Ar, Kr, and Xe by impact of He^+ ions. *Phys. Rev. A* **2010**, *81*, 042709. [CrossRef]

10. Monti, J.M.; Rivarola, R.D.; Fainstein, P.D. Distorted wave theories for dressed-ion-atom collisions with GSZ projectile potentials. *J. Phys. B At. Mol. Opt. Phys.* **2011**, *44*, 195206. [CrossRef]
11. Fainstein, P.D.; Ponce, V.H.; Rivarola, R.D. A theoretical model for ionisation in ion-atom collisions. Application for the impact of multicharged projectiles on helium. *J. Phys. B At. Mol. Opt. Phys.* **1988**, *21*, 287. [CrossRef]
12. Belkic, D.; Gayet, R.; Salin, A. Electron capture in high-energy ion-atom collisions. *Phys. Rep.* **1979**, *56*, 279. [CrossRef]
13. Salin, A. Helium ionisation by high-energy ions at a function of impact parameter and projectile scattering angle. *J. Phys. B At. Mol. Opt. Phys.* **1989**, *223*, 3901. [CrossRef]
14. Rojas, M.F.; Quinto, M.A.; Rivarola, R.D.; Monti, J.M. Dynamic effective charge in the continuum of the CDW-EIS model for ionization in ion–atom collisions: Angular and energy dependence. *J. Phys. B At. Mol. Opt. Phys.* **2023**, *56*, 125201. [CrossRef]
15. Szydlik, P.P.; Green, A.E.S. Independent-particle-model potentials for ions and neutral atoms with $Z < 18$. *Phys. Rev. A* **1974**, *99*, 1885–1894. [CrossRef]
16. Esponda, N.J.; Quinto, M.A.; Rivarola, R.D.; Monti, J.M. Dynamic screening and two-center effects in neutral and partially dressed ion-atom collisions. *Phys. Rev. A* **2022**, *105*, 032817. [CrossRef]
17. McGuire, J.H.; Stolterfoht, N.; Simony, P.R. Screening and antiscreening by projectile electrons in high-velocity atomic collisions. *Phys. Rev. A* **1981**, *24*, 97–102. [CrossRef]
18. Gravielle, M.S.; Miraglia, J.E. Some Nordsieck integral of interest in radiation and atomic collision theories. *Comput. Phys. Commun.* **1992**, *69*, 53–58. [CrossRef]
19. Stolterfoht, N.; DuBois, R.D.; Rivarola, R.D. *Electron Emission in Heavy Ion-Atom Collisions*; Springer: Berlin/Heidelberg, Germany, 1997.
20. Betz, H.D.; Hortig, G.; Leischner, E.; Schmelzer, C.; Stadler, B.; Weihrauch, J. The average charge of stripped heavy ions. *Phys. Lett.* **1966**, *22*, 643–644. [CrossRef]
21. Wang, J.; Reinhold, C.O.; Burgdörfer, J. Electron loss at backward observation angles. *Phys. Rev. A* **1991**, *44*, 7243–7251. [CrossRef]
22. Toburen, L.H.; Wilson, W.E. Differential cross sections for ionization of argon by 0.3–2-MeV He^{2+} and He^{+} ions. *Phys. Rev. A* **1979**, *19*, 2214–2224. [CrossRef]
23. Duncan, M.M.; Menendez, M.G. Ionization of 0.5-MeV H by Ar and a comparison with the H^{-}/Ar system. *Phys. Rev. A* **1979**, *19*, 49–54. [CrossRef]
24. Salvat, F.; Jablonski, A.; Powell, C.J. ELSEPA—Dirac partial-wave calculation of elastic scattering of electrons and positrons by atoms, positive ions and molecules. *Comput. Phys. Commun.* **2005**, *165*, 157–190. [CrossRef]
25. Rudd, M.E.; Risley, J.S.; Fryar, J.; Rolfes, R.G. Angular and energy distribution of electrons from 15- to 150-keV H^0+He collisions. *Phys. Rev. A* **1980**, *21*, 506–514. [CrossRef]
26. Allison, S.K. Experimental Results on Charge-Changing Collisions of Hydrogen and Helium Atoms and Ions at Kinetic Energies above 0.2 kev. *Rev. Mod. Phys.* **1958**, *30*, 1137–1168. [CrossRef]
27. Pivovar, L.I.; Tubayev, V.M.; Novikov, M.T. Electron loss and capture by 200–1500 keV Helium ions in various gases. *Zh. Éksp. Teor. Fiz* **1961**, *41*, 26.
28. Green, A.E.S.; McNeal, R.J. Analytic cross sections for inelastic collisions of protons and hydrogen atoms with atomic and molecular gases. *J. Geophys. Res.* **1971**, *76*, 133–144. [CrossRef]
29. Hvelplund, P.; Pedersen, H.E. Single and double electron loss by fast helium atoms in gases. *Phys. Rev. A* **1974**, *9*, 2434–2439. [CrossRef]
30. Pedersen, E.H.; Heinemeier, J.; Larsen, L.; Mikkelsen, J.V. Electron-loss cross sections for fast, metastable and ground-state helium atoms in gases and metal vapours. *J. Phys. B At. Mol. Phys.* **1980**, *13*, 1167. [CrossRef]
31. Knudsen, H.; Andersen, L.H.; Haugen, H.K.; Hvelplund, P. Electron Loss from Fast One-Electron Ions Colliding with He, N_2, and Ar. *Phys. Script.* **1982**, *26*, 132. [CrossRef]
32. Dmitriev, I.S.; Vorob'ev, N.F.; Konovalova, Z.M.; Nikolaev, V.S.; Novozhilova, V.N.; Teplova, Y.A.; Fainberg, Y.A. Loss and capture of electrons by fast ions and atoms of helium in various media. *Zh. Éksp. Teor. Fiz* **1983**, *84*, 1987–2000.
33. Almeida, D.P.; de Castro Faria, N.V.; Freire, J.F.L.; Montenegro, E.C.; de Pinho, A.G. Collisional formation and destruction of fast negative hydrogen ions in He, Ne, and Ar targets. *Phys. Rev. A* **1987**, *36*, 16. [CrossRef] [PubMed]
34. DuBois, R.D. Multiple ionization in He^{+}–rare-gas collisions. *Phys. Rev. A* **1989**, *39*, 4440–4450. [CrossRef] [PubMed]
35. Radchenko, V.I. Scattering of fast hydrogen particles in gaseous media. *Zh. Éksp. Teor. Fiz* **1994**, *105*, 834–852.
36. Santos, A.C.F.; Melo, W.S.; Sant'Anna, M.M.; Sigaud, G.M.; Montenegro, E.C. Absolute multiple-ionization cross sections of noble gases by He^{+}. *Phys. Rev. A* **2001**, *63*, 062717. [CrossRef]
37. Sarkadi, L.; Herczku, P.; Kovács, S.T.S.; Kövér, A. Multiple ionization of rare gases by hydrogen-atom impact. *Phys. Rev. A* **2013**, *87*, 062705. [CrossRef]
38. Dewangan, D.P.; Walters, H.R.J. Electron loss from H(2s), H(1s), He(11S), He(23S), Li(22S), H- and He- projectiles passing through the inert gases-the free-collision model. *J. Phys. B At. Mol. Phys.* **1978**, *11*, 3983. [CrossRef]
39. Katayama, I.; Berg, G.P.A.; Hurlimann, W.; Martin, S.A.; Meissburger, J.; Oelert, W.; Rogge, M.; Romer, J.G.M.; Tain, J.L.; Zemlo, L.; et al. High-energy electron capture and stripping in gas targets. *J. Phys. B At. Mol. Phys.* **1984**, *17*, L23. [CrossRef]